CrystEngComm

Dynamic Article Links

Cite this: *CrystEngComm*, 2012, **14**, 6910–6915

www.rsc.org/crystengcomm

PAPER

Phase formation in the BaB_2O_4–BaF_2–BaO system and new non-centrosymmetric solid-solution series $Ba_7(BO_3)_{4-x}F_{2+3x}$†

T. B. Bekker,*[a] S. V. Rashchenko,[ab] V. V. Bakakin,[ac] Yu. V. Seryotkin,[ab] P. P. Fedorov,[d] A. E. Kokh[a] and S. Yu. Stonoga[a]

Received 10th July 2012, Accepted 3rd August 2012
DOI: 10.1039/c2ce26122g

Detailed study of the BaB_2O_4–BaF_2–BaO system resulted in the discovery of the new $Ba_7(BO_3)_{4-x}F_{2+3x}$ solid solution belonging to the BaF_2–$Ba_3(BO_3)_2$ section. The distinguishing feature of the crystal structure of $Ba_7(BO_3)_{4-x}F_{2+3x}$ phase is its extensive $(BO_3)^{3-} \leftrightarrow 3F^-$ anionic isomorphic substitution, confirmed by X-ray diffraction study of $Ba_7(BO_3)_{3.51}F_{3.47}$ (x = 0.49) single crystals (space group $P6_3$; a = 11.18241(11) Å, c = 7.23720(8) Å). The area of homogeneity for $Ba_7(BO_3)_{4-x}F_{2+3x}$ solid solution spans between $Ba_7(BO_3)_{3.35}F_{3.95}$ and $Ba_7(BO_3)_{3.79}F_{2.63}$ compositions ($0.21 < x < 0.65$). Also, a new orthorhombic phase with a tentative composition of $Ba_5(BO_3)_3F$ has been identified in XRD powder patterns and indexed with cell parameters a = 7.605 Å, b = 14.843 Å and c = 10.291 Å.

Introduction

Inorganic borates are prospective non-linear optical materials because of their physical properties in the ultraviolet (UV) range of the electromagnetic spectrum.[1–4] Fluoride borates stand out amongst other borates, as they possess much broader areas of transparency with the cut-off edges shifted much further in the aforementioned UV range.[5]

Recently we reported the successful use of ternary phase diagrams for the search of new phases of fluoroborate systems and optimizing conditions for growing the single crystals of these compounds with non-linear optical properties.[6,7]

The BaB_2O_4–BaF_2–BaO ternary system is interesting for both its low temperature modification of barium borate β-BaB_2O_4 and fluoride borates crystal growth. Existing literature data provide sufficient coverage only for BaB_2O_4–BaF_2[8] and BaB_2O_4–BaO[9–11] systems (as a part of the broader BaO–B_2O_3 system). BaB_2O_4–BaF_2 is a quasi-binary system with a eutectic at 760 °C (41 mol% BaB_2O_4 - 59 mol% BaF_2).[8] In contrast, BaB_2O_4–BaO has three individual barium borate compounds: $Ba_5B_4O_{11}$ (melts incongruently at 1170 °C), $Ba_3B_2O_6$ (melts congruently at 1390 °C) and $Ba_4B_2O_7$ (decomposes in the solid state at 1190 °C).[12,13] BaB_2O_4–BaO phase diagram has pertitectic (70 mol% BaO, 1170 °C) and eutectic (61.5 mol% BaO, 910 °C) points[12,13] (Fig. 1). $Ba_5B_4O_{11}$ barium borate crystallizes in the orthorhombic system ($P2_12_12_1$ space symmetry group, a = 9.590, b = 16.66, c = 22.92 Å, PDF 00-058-0115), and earlier[14] this phase was erroneously assigned to a composition of $Ba_2B_2O_5$. Keszler *et al.*[15,16] claimed the existence of two barium fluoride borates: pyrofluoroborate $Ba_5(B_2O_5)_2F_2$[15] and orthofluoroborate $Ba_7(BO_3)_3F_5$.[15,16] $Ba_5(B_2O_5)_2F_2$ was obtained by: (a) melting a stoichiometric pure $BaCO_3$, BaF_2 and B_2O_3 mixture at 1175 K for 1 h followed by its cooling to room temperature, and (b) by precipitation from BaO–BaF_2–B_2O_3 (65.25 : 24.87 : 9.88 mol%)

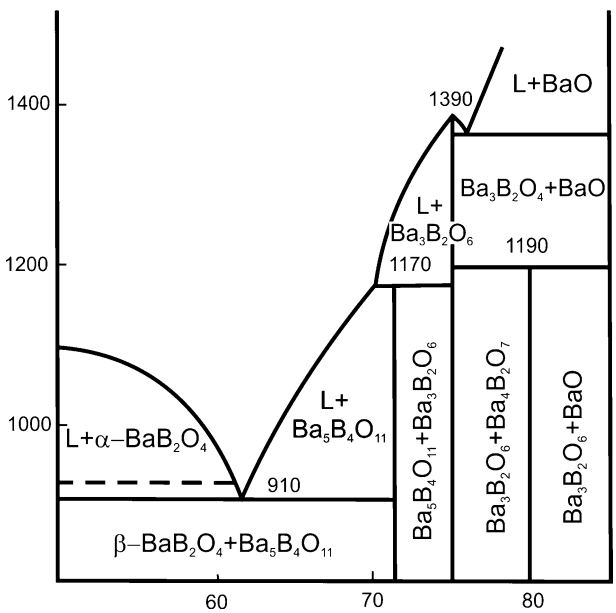

Fig. 1 Phase equilibria along the BaB_2O_4–BaO section.[6]

[a]*Institute of Geology and Mineralogy, Siberian Branch of Russian Academy of Science, 630090, Novosibirsk, Russia. E-mail: t.b.bekker@gmail.com*
[b]*Novosibirsk State University, 630090, Novosibirsk, Russia*
[c]*Institute of Inorganic Chemistry, Siberian Branch of Russian Academy of Sciences, 630090, Novosibirsk, Russia*
[d]*General Physics Institute, Russian Academy of Science, 119991, Moscow, Russia*

† CCDC 891832. For crystallographic data in CIF or other electronic format see DOI: 10.1039/c2ce26122g

melt. In the latter case, $Ba_5(B_2O_5)_2F_2$ was co-precipitated with $Ba_7(BO_3)_3F_5$ phase. The authors determined that $Ba_5(B_2O_5)_2F_2$ crystallizes in a monoclinic system (*C*2/*c* space symmetry group; a = 20.726, b = 7.115, c = 8.589 Å, β = 95.05°, (PDF 04-009-5031) and melts congruently at about 1040 K, whereas $Ba_7(BO_3)_3F_5$ has a trigonal lattice (*P*31*c* space group; a = 11.208(5), c = 7.250(2) Å, R_w = 0.075). However, Keszler *et al.* papers[15,16] appear to be the only data available for the BaB_2O_4–BaF_2–BaO system. Therefore, we carried out additional studies of BaB_2O_4–BaF_2–BaO system, and present to the reader of this paper our data for BaB_2O_4–BaF_2–BaO system subsolidus area as well as the crystal structure of a new barium fluoride borate formed in this system.

Experimental

Samples to study phase equilibria in the subsolidus area of BaB_2O_4–BaF_2–BaO system (usually *ca.* 5.0 g) were prepared in a platinum crucible in furnace with periodic grinding under air. Specimen heating was controlled with an accuracy of $\pm$0.1 °C using an Eurotherm 2604. High purity (99.99 wt.%) BaF_2, $BaCO_3$ and BaB_2O_4 were used as starting materials (the latter was synthesized from H_3BO_3 and $BaCO_3$[17]). Phase composition of the products of the solid phase syntheses were studied by X-ray diffraction with the use of ARL X′TRA powder X-ray diffractometer (Cu-Kα, Bragg-Brentano geometry). A sample was considered under equilibrium if its X-ray diffraction (XRD) patterns remained unchanged after two consecutive annealing cycles.

Because $Ba_5(B_2O_5)_2F_2$ melts at about 767 °C,[15] and temperatures of both binary and ternary invariant points involving this compound are lower than its melting temperature, solid phase preparations of the samples with compositions within BaB_2O_4–BaF_2–$Ba_5B_4O_{11}$ subsystem were carried out at temperatures not exceeding 730 °C.

The single crystals in the BaB_2O_4–BaF_2–BaO system were grown on a platinum wire loop in air. The batch (*ca.* 30 g) with the composition BaB_2O_4 : BaF_2 : BaO = 25 : 35 : 45 mol% was melted in a platinum crucible (40 mm in diameter). The heating rate was 25 °C h^{-1}; the maximum heating temperature was 1050 °C. The liquidus temperature of *ca.* 1030 °C was determined by visual polythermal analysis. At this temperature a platinum wire loop was placed into the central part of the melt surface to induce spontaneous crystallization. After the latter process began, the melt was cooled at the rate of 2 °C day^{-1} for 4 days in order to increase the crystal size.

Results and discussion

XRD patterns of prepared $Ba_5(B_2O_5)_2F_2$ specimens coincided with PDF 04-009-5031. Detailed X-ray diffraction studies of the samples, corresponding to the compositions of $Ba_5(B_2O_5)_2F_2$–BaF_2, $Ba_5(B_2O_5)_2F_2$–BaB_2O_4, $Ba_5(B_2O_5)_2F_2$–$Ba_5B_4O_{11}$ and $Ba_5B_4O_{11}$–BaF_2 sections, indicated that the reaction products contained only $Ba_5(B_2O_5)_2F_2$ and BaF_2, $Ba_5(B_2O_5)_2F_2$ and BaB_2O_4, $Ba_5(B_2O_5)_2F_2$ and $Ba_5B_4O_{11}$, $Ba_5B_4O_{11}$ and BaF_2 phases, respectively. In other words, all of the above sections are quasi-binary for the temperatures below the solidus one.

Taking into account the existence of $Ba_5(B_2O_5)_2F_2$ in the BaB_2O_4–BaF_2–$Ba_5B_4O_{11}$ subsystem, we considered triangulation of the latter by its splitting into three secondary phase triangles: BaB_2O_4–$Ba_5(B_2O_5)_2F_2$–BaF_2, BaB_2O_4–$Ba_5B_4O_{11}$–$Ba_5(B_2O_5)_2F_2$, and $Ba_5(B_2O_5)_2F_2$–$Ba_5(B_2O_5)_2F_2$–BaF_2 (Fig. 2). Our synthetic experiments (Table 1) repeatedly confirmed the correctness of this suggestion.

Stoichiometry of "$Ba_7(BO_3)_3F_5$", described by Keszler *et al.*[16] (62.5 mol% BaF_2 and 37.5 mol% $Ba_3(BO_3)_2$), falls into BaF_2–$Ba_3(BO_3)_2$ section of the BaB_2O_4–BaF_2–BaO system. We prepared sample of this composition and repeatedly annealed it at 700, 750, 800, 850, 900 and 920 °C for 1 day at each temperature (Table 2, Fig. 3).

X-Ray diffraction patterns of the sample with exact "$Ba_7(BO_3)_3F_5$" stoichiometry (Fig. 3) contain strong peaks of BaF_2 cubic phase. The latter means that there is no such individual "$Ba_7(BO_3)_3F_5$" phase. However, the remaining lines were easily indexed in hexagonal system with a = b = 11.174 Å and c = 7.245 Å parameters, similar to the ones proposed by Keszler *et al.*[16] for the aforementioned "$Ba_7(BO_3)_3F_5$". We succeeded in our attempts to obtain an individual hexagonal phase with the above parameters by decreasing the amount of BaF_2 in the starting batches (Table 2, Fig. 3): samples "2" contained almost pure hexagonal phase with trace amounts of BaF_2, and samples "3" and "4" had only hexagonal phase reflections in their X-ray diffraction patterns. The existence of the individual phase in such a broad range of compositions (points "2", "3" and "4") unequivocally indicates anionic isomorphism, *e.g.*, $(BO_3)^{3-} \leftrightarrow 3F^-$.[18–20]

However, samples with the chemical composition "5" (Table 2, Fig. 3) contained—in addition to the above hexagonal phase—another phase with X-ray diffraction pattern indexed in orthorhombic system (a = 7.605; b = 14.843 and c = 10.291 Å).

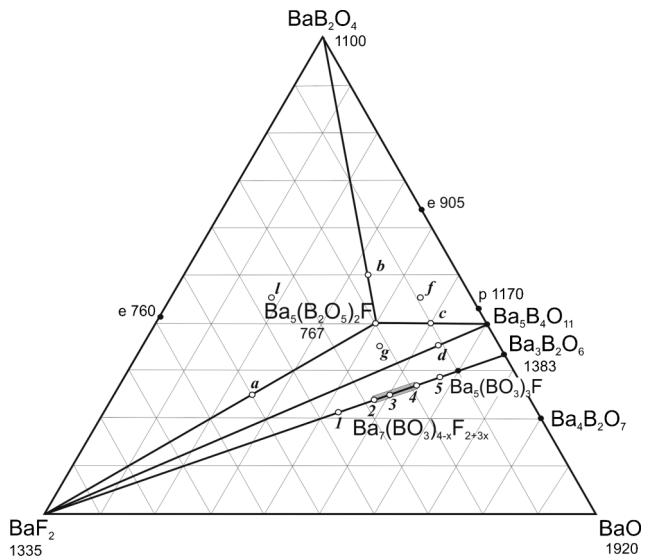

Fig. 2 Concentration triangle of the BaB_2O_4–BaF_2–BaO system and the suggested triangulation scheme of the BaB_2O_4-$Ba_5B_4O_{11}$–BaF_2 subsystem. "1" to "5" and "*a*" to "*l*" circles represent the prepared samples (Tables 1 and 2). Numbers next to chemical formulas and/or filled circles with letters "*p*" and "*e*" correspond to melting, peritectic and eutectic temperatures.

Table 1 Solid state synthesis of the samples with compositions within BaB_2O_4–$Ba_5B_4O_{11}$–BaF_2 subsystem

Composition, mol (%)	Annealing T/°C	Annealing time, day	Obtained phases (XRD)
$Ba_5(B_2O_5)_2F_2$	700	1	
40 BaB_2O_4–40 BaO–20 BaF_2	750	2	$Ba_5(B_2O_5)_2F_2$
Sample "*a*"			
25 $Ba_5(B_2O_5)_2F_2$–75 BaF_2	700	1	
(25 BaB_2O_4–25 BaO–50 BaF_2)	730	2	$Ba_5(B_2O_5)_2F_2$ + BaF_2
Sample "*b*"			
50 $Ba_5(B_2O_5)_2F_2$–50 BaB_2O_4	700	1	
(50 BaB_2O_4–33 BaO–17 BaF_2)	730	2	$Ba_5(B_2O_5)_2F_2$ + BaB_2O_4
Sample "*c*"			
33.3 $Ba_5(B_2O_5)_2F_2$–66.7 $Ba_5B_4O_{11}$	700	1	
(40 BaB_2O_4–50 BaO–10 BaF_2)	730	2	$Ba_5(B_2O_5)_2F_2$ + $Ba_5B_4O_{11}$
Sample "*d*"	700	1	
75.5 $Ba_5B_4O_{11}$–24.5 BaF_2	750	1	
(35.5 BaB_2O_4–53 BaO–11.5 BaF_2)	800	2	BaF_2 + $Ba_5B_4O_{11}$
Sample "*f*"	700	1	
46 BaB_2O_4–28 BaO–36 BaF_2	730	2	$Ba_5(B_2O_5)_2F_2$ + BaB_2O_4 + BaF_2
Sample "*f*"	700	1	
46 BaB_2O_4–9 BaO–45 BaF_2	730	2	$Ba_5(B_2O_5)_2F_2$ + BaB_2O_4 + $Ba_5B_4O_{11}$
Sample "*g*"	700	1	
35 BaB_2O_4–43 BaO–22 BaF_2	730	2	$Ba_5(B_2O_5)_2F_2$ + $Ba_5B_4O_{11}$ + BaF_2

[a] Note: Compositions of the samples are marked in Fig. 2 with the corresponding characters.

Table 2 Solid state synthesis of the samples with compositions on BaF_2–$Ba_3(BO_3)_2$ section

Composition, mol (%)	Annealing T/°C	Annealing time, day(s)	Obtained phases (XRD)
Sample "1" '$Ba_7(BO_3)_3F_5$'	700, 750, 800, 850, 900, 920	1 day at each step	BaF_2 + $Ba_7(BO_3)_{4-x}F_{2+3x}$ hexagonal phase
62.5 BaF_2–37.5 $Ba_3(BO_3)_2$			
Sample "2"	750, 850, 900, 920	1 day at each step	$Ba_7(BO_3)_{4-x}F_{2+3x}$ hexagonal phase + trace amount of BaF_2
54 BaF_2–46 $Ba_3(BO_3)_2$			
Sample "3"	750, 850, 900, 920	1 day at each step	$Ba_7(BO_3)_{4-x}F_{2+3x}$ hexagonal phase
50 BaF_2–50 $Ba_3(BO_3)_2$			
Sample "4"	750, 850, 900, 920	1 day at each step	$Ba_7(BO_3)_{4-x}F_{2+3x}$ hexagonal phase
41 BaF_2–59 $Ba_3(BO_3)_2$			
Sample "5" '$Ba_7(BO_3)_4F_2$'	750, 850, 900, 920	1 day at each step	$Ba_7(BO_3)_{4-x}F_{2+3x}$ hexagonal phase + $Ba_5(BO_3)_3F$ orthorhombic phase (tentative composition)
33 BaF_2–67 $Ba_3(BO_3)_2$			

[a] Note: Compositions of the samples are marked in Fig. 2 with the corresponding numbers.

The latter is probably $Ba_5(BO_3)_3F$ phase isostructural to the known strontium fluoroborate $Sr_5(BO_3)_3F$ (a = 7.220 b = 14.092 Å and c = 9.810 Å).[21]

We obtained crystalline aggregates (Fig. 4) by spontaneous crystallization on a platinum loop from the melt with BaB_2O_4 : BaF_2 : BaO = 25 : 35 : 45 mol% composition. X-Ray diffraction pattern of the crystals coincided with the hexagonal phase, described above. A high-quality single crystal sample with dimensions of 0.12 × 0.11 × 0.06 mm was selected with the use of a polarizing microscope for further investigation. X-Ray diffraction data were collected on Oxford Diffraction Gemini R Ultra single-crystal diffractometer (CCD-detector, graphite-monochromatized Mo-Kα radiation) using the ω-scan technique with scan width of 0.75° per frame. Data reduction was performed with Oxford Diffraction CrysAlisPro software and the space group was selected as the most appropriate one on the basis of systematic absences and intensities of reflections. SHELX-97 software[22] (WinGX suite[23]) was used for structure solution and refinement.

The details of data collection and structure refinement are summarized in Table 3. All structural data including atomic coordinates, isotropic and equivalent displacement parameters and refined site occupancies are listed in Table 4.

The solved structure corresponds to the same structural type as $Ba_{4-x}Sr_{3+x}(BO_3)_{4-y}F_{2+3y}$ solid-solution series described earlier.[18] The most appropriate representation of the structure is cation sublattice with anions filling the cavities as per approach suggested for alkali-earth borates by A. Vegas.[24] The cation sublattice contains nets perpendicular to the c-axis; each net contains triangular, rectangular and centered hexagonal loops (Fig. 5 and 6), thus corresponding to the semi-regular net type described by Wells.[25] The nets are multiplied by 6_3 axes passing through triangular loops. Fluorine F1 anions occupy octahedral cavities formed by two triangular loops (Fig. 7). They are shifted along the c-axis toward three basal Ba atoms. $(BO_3)^{3-}$ groups, containing B1, O1, O2 and O3 atoms, are located inside three-capped trigonal prisms (Fig. 7). Large cavities between hexagonal and trigonal loops are filled with "4X" anionic groups (trigonal pyramids located on the threefold axis, Fig. 8) that appear to be the distinguishing feature of the structure. Each triangular face of this pyramid (except the basal one) may be occupied either by $3F^-$ or by $(BO_3)^{3-}$ groups, giving statistical

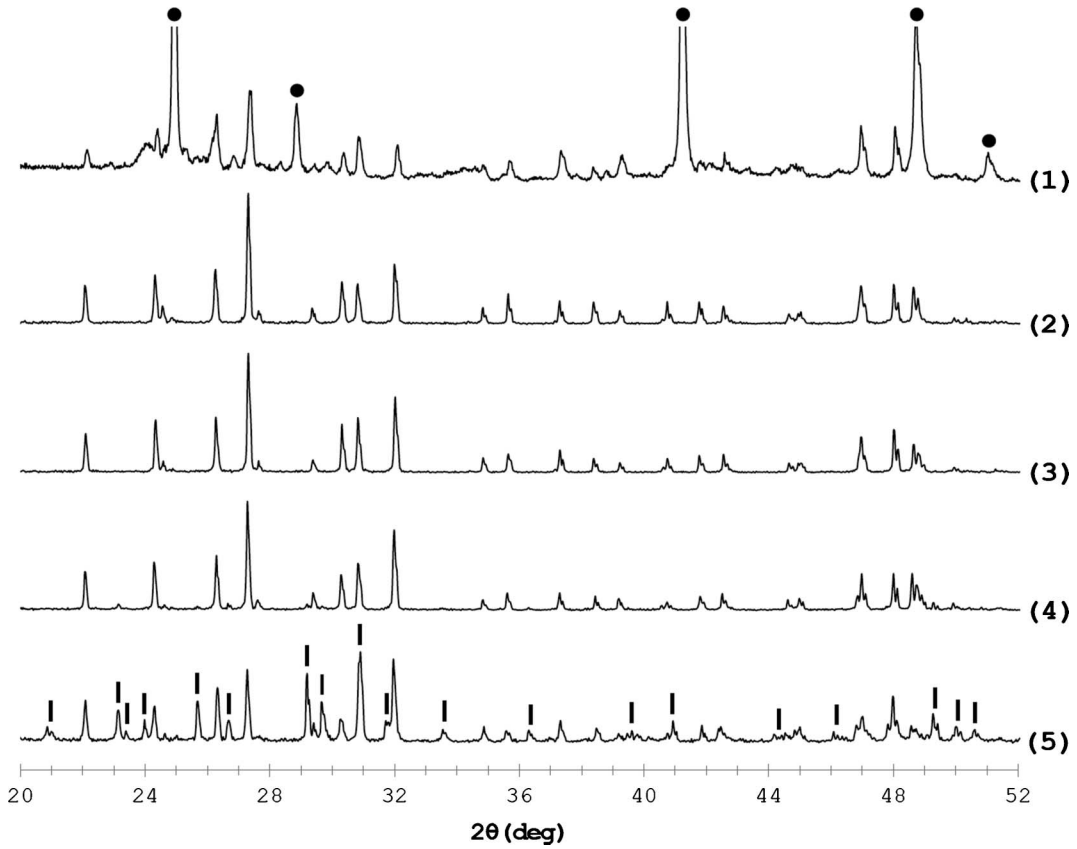

Fig. 3 X-ray diffraction patterns of solid-state reaction products in BaF_2–$Ba_3(BO_3)_2$ system: samples 1–5 correspond to the compositions listed in Table 2 with the same numbers. Circles and strokes mark peaks of BaF_2 and orthorhombic phase (probably, $Ba_5(BO_3)_3F$), respectively. Unmarked peaks correspond to $Ba_7(BO_3)_{4-x}F_{2+3x}$ phase.

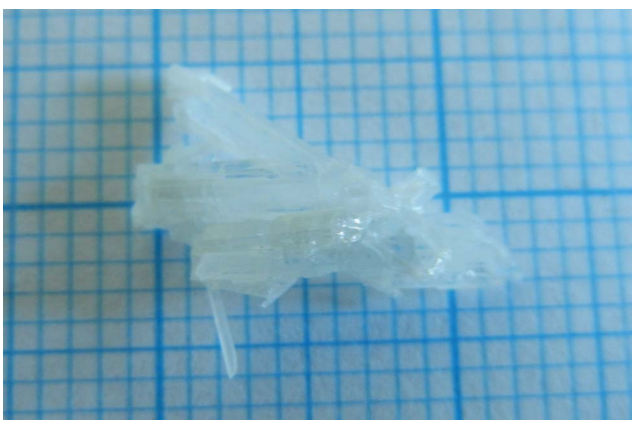

Fig. 4 $Ba_7(BO_3)_{4-x}F_{2+3x}$ crystal aggregate obtained from BaB_2O_4 : BaF_2 : BaO = 25 : 35 : 45 mol% batch.

distribution of $(BO_3)F$ and 4F pyramids over the crystalline lattice. Such isomorphic substitution $(BO_3)^{3-} \leftrightarrow 3F^-$ has been reported earlier for a number of compounds,[18–20] for which we consider it to be a specific feature of the crystal structure. To determine the degree of anionic isomorphic substitution in the grown single crystals, we refined the occupancies of statistically populated sites using charge balance restraints; refined composition was $Ba_7(BO_3)_{3.51}F_{3.47}$ (x = 0.49).

Table 3 Parameters of single-crystal data collection and structure refinement

Refined stoichiometry	$Ba_7(BO_3)_{3.51}F_{3.47}$ (Z = 2)
Formula weight	1233.73
Space group	$P6_3$ (#173)
a/Å	11.18241(11)
c/Å	7.23720(8)
Calculated density/g cm^{-3}	5.228
Absorption coefficient μ/mm^{-1}	17.377
F(000)	1050
θ range/°	2.10–37.21
hkl limits	$-18 \leqslant h \leqslant 18$; $-18 \leqslant k \leqslant 18$; $-12 \leqslant l \leqslant 12$
Measured reflections	27 864
Unique reflections	2665
Reflections with $I > 2\sigma(I)$	2622
R_{int}	0.0450
Refined parameters	79
Flack parameter	0.20(8)
R factors ($I > 2\sigma(I)$)	R_1 = 0.0251; wR_2 = 0.0545
R factors (all data)	R_1 = 0.0258; wR_2 = 0.0548
Residual electron density/e Å^{-3}	max 2.097; min −2.500; average 0.243

It should be mentioned that oxygen and fluorine atoms occupy different positions in the vertices of "4X" pyramids (Fig. 8): O-atoms of $(BO_3)^{3-}$ anions are located closer to each other (*ca.* 2.5 Å) than corresponding F-atoms that have a larger distance

Table 4 Positional parameters of $Ba_7(BO_3)_{3.51}F_{3.47}$ structure

	Occupancy	*x*	*y*	*z*	U_{eq}/U_{iso}	
Ba1	1	0.87413(5)	0.73882(3)	0.04356(7)	0.01663(6)	
Ba2	0.660(5)	0.07140(10)	0.54223(10)	0.22308(9)	0.00955(15)	
Ba2′	0.340(5)	0.0467(2)	0.5188(2)	0.1901(2)	0.0116(3)	
Ba3	1	2/3	1/3	0.29522(9)	0.01391(8)	
O1	1	0.6972(5)	0.8549(7)	0.1583(6)	0.0226(8)	
O2	1	0.7066(6)	0.5999(6)	0.3839(7)	0.0179(10)	
O3	1	0.6062(5)	0.6854(5)	0.9210(8)	0.0179(9)	
B1	1	0.6343(5)	0.8154(9)	0.9866(7)	0.0121(7)	
F1	1	0	0	0.9001(10)	0.0297(13)	
X1O	0.510(8)	1/3	2/3	0.215(2)	0.021(3)	
X1F	0.490(8)	1/3	2/3	0.1429(16)	0.0115(16)	
X2O	0.340(5)	0.8000(16)	0.4515(16)	0.993(2)	0.019(3)	
X2F	0.660(5)	0.8373(7)	0.4918(7)	0.0354(11)	0.0217(11)	
B2	0.170(3)	0.681(3)	0.392(3)	0.904(3)	0.004(4)	
	U_{11}	U_{22}	U_{33}	U_{23}	U_{13}	U_{12}
Ba1	0.01163(14)	0.01778(12)	0.02117(12)	0.00411(11)	0.00220(17)	0.00787(13)
Ba3	0.01097(11)	0.01097(11)	0.01981(19)	0	0	0.00548(6)
O1	0.030(2)	0.018(2)	0.0155(16)	–0.003(2)	–0.0079(14)	0.010(2)
O2	0.018(2)	0.023(2)	0.0165(19)	–0.0038(16)	–0.0038(16)	0.0125(19)
O3	0.018(2)	0.0080(17)	0.028(2)	–0.0084(18)	–0.0017(17)	0.0070(16)
B1	0.0086(17)	0.013(3)	0.0129(17)	0.005(3)	0.0026(14)	0.004(2)
F1	0.030(2)	0.030(2)	0.030(3)	0	0	0.0148(10)

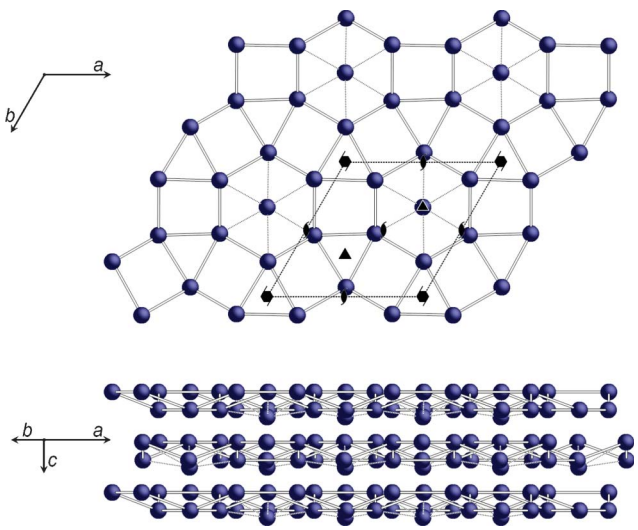

Fig. 5 Cation sublattice of $Ba_7(BO_3)_{4-x}F_{2+3x}$ structure: a single net (top), and nets sequence (bottom). The unit cell is shown with dotted line; all spheres represent Ba^{2+} cations.

between each other (*ca.* 3.3 Å). As a result of such geometrical difference between $(BO_3)F$ and 4F types of "4X" pyramids neighbouring barium cation positions also become different (they are labelledd as Ba2 and Ba2′ in Fig. 8).

As a result of observed $(BO_3)^{3-} \leftrightarrow 3F^-$ isomorphic substitution, the general formula of studied solid solution may be presented as $Ba_7(BO_3)_{4-x}F_{2+3x}$. Data of our synthetic experiments (Table 2, Fig. 2) indicate the homogeneity of $Ba_7(BO_3)_{4-x}F_{2+3x}$ solid solution between $Ba_7(BO_3)_{3.35}F_{3.95}$ (sample "2") and $Ba_7(BO_3)_{3.79}F_{2.63}$ (sample "4") compositions, *i.e.*, for $0.21 < x < 0.65$. Fitting and indexing of the corresponding X-ray diffraction patterns of these samples showed only a very slight change for the crystal lattice parameters.

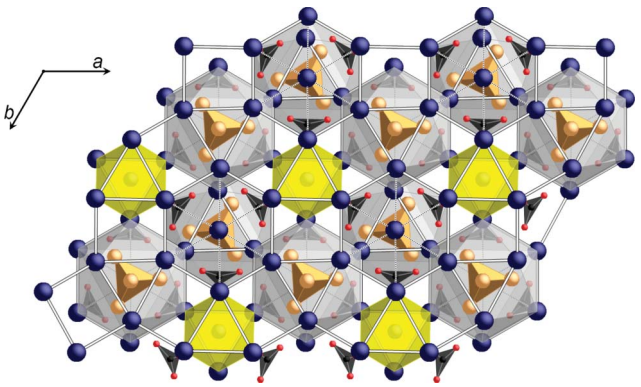

Fig. 6 $Ba_7(BO_3)_{4-x}F_{2+3x}$ structure. Anion-filled cation sublattice (dark blue spheres represent Ba^{2+} cations). F1 fluorine atoms occupies octahedral cavities (yellow). "4X" anionic groups are shown as orange pyramids inside gray polyhedra; $(BO_3)^{3-}$ anions are marked as black triangles.

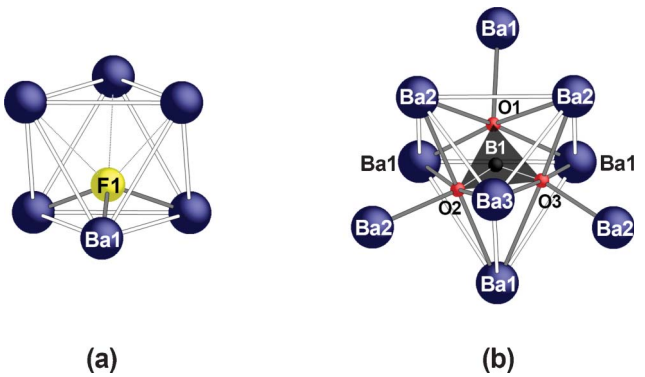

Fig. 7 The anion-centered polyhedra in the $Ba_7(BO_3)_{4-x}F_{2+3x}$ structure: the $(Ba1)_6$ octahedron (a), and $(Ba1)_4(Ba2)_4Ba3$ three-capped trigonal prism (b).

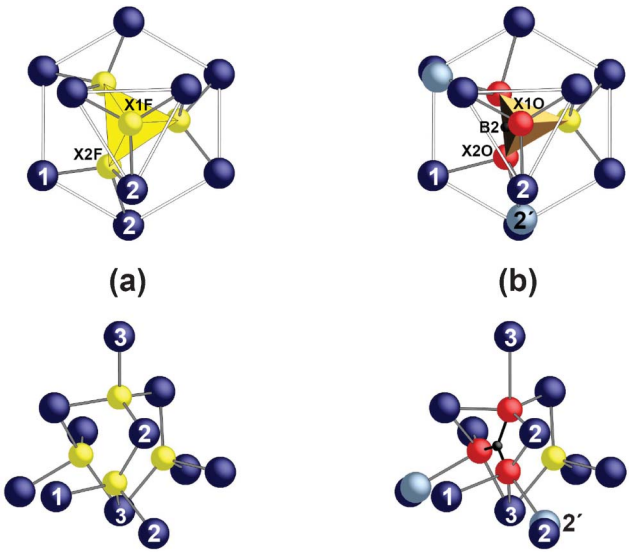

Fig. 8 The coordination of "4X" anionic group in their 4F (a) and $(BO_3)F$ (b) realizations. Yellow spheres represent fluorine atoms. Boron and oxygen atoms in $(BO_3)^{3-}$ groups are shown as black and red spheres with black B–O bonds. Barium cation sites Ba1, Ba2, and Ba3 are shown as dark blue spheres with corresponding numbers, and two Ba2′ sites, shifted towards oxygen atoms, are coloured in light blue with the corresponding number.

Theoretically, composition of $Ba_7(BO_3)_{4-x}F_{2+3x}$ solid solution could span up to its hypothetical terminal compositions $Ba_7(BO_3)_4F_2$ ($x = 0$) and $Ba_7(BO_3)_3F_5$ ($x = 1$). Keszler *et al.*[16] assigned the last stoichiometry to the obtained sample, but—according to our data presented in this paper—both terminal stoichiometries '$Ba_7(BO_3)_4F_2$' (Table 2, sample "5") and '$Ba_7(BO_3)_3F_5$' (Table 2, sample "1") do not exist as individual phases.

Conclusions

Detailed study of the BaB_2O_4–BaF_2–BaO system resulted in the discovery of the new $Ba_7(BO_3)_{4-x}F_{2+3x}$ solid solution with broad anionic isomorphism $(BO_3)^{3-} \leftrightarrow 3F^-$, confirmed by X-ray diffraction study of $Ba_7(BO_3)_{3.51}F_{3.47}$ ($x = 0.49$) single crystals (space group $P6_3$; $a = 11.18241(11)$ Å, $c = 7.23720(8)$ Å. Also, a new orthorhombic phase with a tentative composition of $Ba_5(BO_3)_3F$ has been identified in XRD powder patterns and indexed with cell parameters $a = 7.605$, $b = 14.843$ Å and $c = 10.291$ Å. Further research on the BaB_2O_4–BaF_2–BaO system is in progress.

Acknowledgements

Authors are very grateful to Dr. A. Popov and Dr. R. Simoneaux for their help in manuscript preparation.

References

1 C. T. Chen, Y. C. Wu, A. D. Jiang, G. M. You, R. K. Li and S. J. J. Lin, *J. Opt. Soc. Am. B*, 1989, **6**, 616–621.
2 T. Sasaki, Y. Mori, M. Yoshimura, Y. K. Yap and T. Kamimura, *Mater. Sci. Eng., R*, 2000, **30**(1–2), 1–54.
3 Z. S. Lin, J. Lin, Z. Z. Y. C. Wang, N. Wu, C. T. Ye, R. K. Chen and J. Li, *J. Phys.: Condens. Matter*, 2001, **13**, R369–R384.
4 P. P. Fedorov, A. E. Kokh and N. G. Kononova, *Russ. Chem. Rev.*, 2002, **71**(8), 651–671.
5 B. C. Wu, D. I. Tang, N. Ye and C. T. Chen, *Opt. Mater.*, 1996, **5**, 105–109.
6 P. P. Fedorov, N. G. Kononova, A. E. Kokh and T. B. Bekker, *J. Cryst. Growth*, 2008, **310**(7–9), 1943–1949.
7 T. B. Bekker, P. P. Fedorov and A. E. Kokh, *Cryst. Growth Des.*, 2012, **12**(1), 129–134.
8 T. Bekker, A. Kokh and P. Fedorov, *CrystEngComm*, 2011, **13**, 3822–3826.
9 E. M. Levin and H. F. J. McMurdie, *Res. Nat. Bur. Stand.*, 1949, **42**, 131–137.
10 V. Nikolov and P. J. Peshev, *J. Solid State Chem.*, 1992, **96**, 48–52.
11 J. L. Stone, A. Keszler, G. Aka, A. Kahn-Harari and T. A. Reynolds, *Proc. SPIE–Int. Soc. Opt. Eng.*, 2001, **4268**, 175–179.
12 A. E. Kokh, N. G. Kononova, T. B. Bekker, Y. F. Kargin, N. G. Furmanova, P. P. Fedorov, S. V. Kusnetsov and E. A. Tkachenko, *J. Russ. Inorg. Chem.*, 2005, **50**(11), 1749–1753.
13 N. G. Furmanova, B. A. Maksimov, V. N. Molchanov, A. E. Kokh, N. G. Kononova and P. P. Fedorov, *Crystallogr. Rep.*, 2006, **51**(2), 219–224.
14 K. Hubner and H. Neues, *Jahduch fur Mineralogie Monatsh.*, 1969, **B 111**, S.335.
15 T. Alekel and D. A. J. Keszler, *J. Solid State Chem.*, 1993, **106**, 310–316.
16 D. A. Keszler, A. Akella, K. I. Schaffers and T. A. Alekel, *Materials Research Society Symposia Proceedings*, 1994, 15–22.
17 N. G. Kononova, A. E. Kokh, *Patent RU N 2195520*, Bull., 2002, 36, (in Russian).
18 S. V. Rashchenko, T. B. Bekker, V. V. Bakakin, Yu. V. Seryotkin, V. S. Shevchenko, A. E. Kokh and S. Yu. Stonoga, *Cryst. Growth Des.*, 2012, **12**(6), 2955–2960.
19 E. Antic-Fidancev, G. Corbel, N. Mercier and M. J. Leblane, *J. Solid State Chem.*, 2000, **153**, 270–274.
20 A. A. Brovkin, I. V. Rozdestvenskaya and E. A. Rykova, *Second Russian National Crystal Chemical Conference Proceedings*, 2000http://margot.icp.ac.ru/conferences/old/NCCC/abstracts/Brovkin.html.
21 T. Alekel and D. A. Keszler, *Inorg. Chem.*, 1993, **32**, 101–105.
22 G. M. Sheldrick, *Acta Crystallogr., Sect. A: Found. Crystallogr.*, 2007, **64**, 112–122.
23 L. J. J. Farrugia, *J. Appl. Crystallogr.*, 1999, **32**, 837–838.
24 A. Vegas, *Acta Crystallogr., Sect. C: Cryst. Struct. Commun.*, 1985, **41**, 1689–1690.
25 A. F. Wells, *Structural Inorganic Chemistry*, 1975, 1095.